Thermal aging of heteroatom substituted Keggin type aluminum oxo polycation solutions: Aggregation behavior and impacts on dissolved organic carbon and turbidity removal

Mohammad Shohel[*1], Jack A. Smith[1], Margaret A. Carolan[1,2], Tori Z. Forbes[*1]

[1]Department of Chemistry, University of Iowa, Iowa City, IA-52242
[2]Department of Civil and Environmental Engineering, University of Iowa, Iowa City, IA-52242
*Corresponding authors: tori-forbes@uiowa.edu, mohammad-shohel@uiowa.edu

Abstract

Coagulation processes within water treatment plays an important role in contaminant removal and aluminum-oxo Keggin polycations are proved to be an effective coagulating agents. Previous work demonstrated that heteroatom substitution within the Keggin-type polycation ε-Al$_{13}$ to form ε-GaAl$_{12}$ and ε-GeAl$_{12}$ can enhance removal of bacteria, DOC, and turbidity from wastewater. Additional hydrolysis of the ε-Al$_{13}$ species to form larger Al$_{30}$ species has also been shown to improve coagulation, but this aspect has not been evaluated for the ε-GaAl$_{12}$ and ε-GeAl$_{12}$ systems. In the current study, hydrolysis of ε-Al$_{13}$, ε-GaAl$_{12}$ and ε-GeAl$_{12}$ was promoted through hydrothermal aging to evaluate the overall solution stability/behavior and water treatment efficiency. Turbidity measurement of aged solution indicated that Ga substituted aluminum-oxo Keggin polycations remain stable in solution and DLS studies demonstrated greater diversity in particle sizes within the system. Additional thermogravimetric analyses of metal hydroxide precipitates formed from the aging studies indicate that the GaAl$_{12}$ system behaves more like an amorphous Al(OH)$_3$ phase, which has higher solubility than other aluminum hydroxide phases. Hydrothermal aging did not significantly change %DOC removal as all solution showed high efficiency for removal across a range of pH values. GaAl$_{12}$ solutions demonstrated good turbidity removal efficiency in all pH range, with enhanced performance at pH 5. The study suggests that larger, relatively stable oligomers do exist within the aged GaAl$_{12}$ solutions that may contribute to enhanced contaminant removal in a similar manner to what is observed within the PACl-Al$_{30}$ coagulant.

Keywords: Wastewater treatment, Coagulation, Aluminum-oxo polycation, Heteroatom, Keggin

Introduction

Coagulation and flocculation are crucial processes for wastewater treatment and rely on the addition of chemical agents to remove impurities from the water. Wastewater contains dissolved and suspended particles that must be removed before recharge into natural waters. The suspended particles are typically composed of clay, natural organic matter, etc., whereas the dissolved component contains a range of molecular inorganic (i.e. Na^+, K^+, Ca^{2+}, PO_4^{3-}, CO_3^{2-}, Cl^-) and organic species, including some trace contaminants (i.e. heavy metals herbicides, pesticides, pharmaceuticals) that are harmful to human health and the natural environment. To remove these species, coagulation agents are added to the water to aggregate and/or flocculate the suspended and dissolved particles. These flocculants can physically be separated within the water treatment facility to remove them before recharge.

Over the past 20 years, efforts to improve coagulation agents have turned away from simple metal salts and towards partially-hydrolyzed polyaluminum nanoclusters. The most widely used coagulation agents are based upon the hydrolysis Al^{3+} and Fe^{3+} salts, such as alum and ferric chloride. Addition of these metals to water at a circumneutral pH results in hydrolysis of the metal cation to larger nanoscale polyaluminum species and can be used for aggregation of the flocculant.[1, 2] Structurally, these polyaluminum cations are based upon the formation of 1-2 nm Keggin-type clusters, with the exact solution speciation dependent on synthetic conditions. The Keggin-type structural topology consists of a central tetrahedrally coordinated Al^{3+} cation surrounded by twelve additional Al^{3+} in octahedral coordination to form ~1 nm size $[AlO_4Al_{12}(OH)_{24}(H_2O)_{12}]^{7+}$ (Al_{13}) species.[3] Initially the Al^{3+}-bearing solutions undergo partial hydrolysis to form the ε-Al_{13} isomer and additional aging results in the creation of Al_{13} isomers (δ-

59   Al$_{13}$, γ-Al$_{13}$) and larger ~2 nm oligomers)[Al$_2$(μ$_4$-O$_8$)(Al$_{24}$(μ$_2$-OH)$_{50}$(H$_2$O)$_{20}$]$^{12+}$ (Al$_{26}$),

60   [Al$_{30}$O$_8$(OH)$_{56}$(H$_2$O)$_{24}$]$^{18+}$ (Al$_{30}$) and [Al$_{32}$O$_8$(OH)$_{60}$(H$_2$O)$_{28}$(SO$_4$)$_2$]$^{16+}$ (Al$_{32}$)).[3-6]

61   Polyaluminum coagulants are currently on the market (i.e. PAC, PACI, and ACH) and

62   demonstrate higher performance compared to alum and ferric chloride. Each polyaluminum

63   nanocluster possesses a high positive charge that can more effectively attract the negatively

64   charged contaminants to form neutral flocculants and also physically trap neutral or cationic

65   species in the aggregation process. This means the partially hydrolyzed coagulant is effective at

66   lower dosages, has a wider operational range at different condition (pH, temperature, colloids

67   concentration, etc.), and better floc formation.[7-10] For example, Mertens *et al.* 2012 reported PACl

68   coagulants with higher Al$_{30}$ content performed best at removing As(V) from natural well water

69   (20-2300 µg/L) to levels that are below the World Health Organization guideline of 10 µg/L.[11] In

70   addition, polyaluminum based coagulants have also shown enhanced performance for treatment of

71   natural organic matter, bacteriophage and clay particles from wastewater.[12-16] Very recently, Wang

72   and co-workers have also shown the use of polyaluminum coagulants in removing dyes, antibiotics

73   and even model microplastics from wastewater.[17, 18]

74   Heteroatom substitution of the polyaluminum nanoclusters results in subtle variabilities of

75   the surface chemistry and can give rise to improved coagulation. Both Ga^{3+} and Ge^{4+} readily

76   substitute into the central tetrahedral site within the ε-Al$_{13}$ topology to create the

77   [GaO$_4$Al$_{12}$(OH)$_{24}$(H$_2$O)$_{12}$]$^{7+}$ (GaAl$_{12}$) and [GeO$_4$Al$_{12}$(OH)$_{24}$(H$_2$O)$_{12}$]$^{7+}$ (GeAl$_{12}$) species,

78   respectively.[19, 20] Coagulation behavior of the ε-GaAl$_{12}$ and ε-GeAl$_{12}$ species was performed by

79   Stewart *et al.* and the authors demonstrated the importance of this single atom substitution in ε-

80   Al$_{13}$. Contaminant removal efficacy of bacteriophage, Cryptosporidium, and dissolved organic

81 carbon (DOC) for heteroatom substituted ε-Keggin isomers indicated that a trend where the

82 polyaluminum clusters could be ranked $\varepsilon\text{-GaAl}_{12} > \varepsilon\text{-Al}_{13} > \varepsilon\text{-GeAl}_{12}$.

83   While the performance of polyaluminum species in PACl coagulation behavior has been

84 evaluated, less is known regarding clusters with heteroatomic substitution. The study by Stewart

85 *et al.* focused solely on $\varepsilon\text{-Al}_{13}$ and related $\varepsilon\text{-MAl}_{12}$ (M = Ga^{3+} and Ge^{4+}) clusters in the removal of

86 suspended and dissolved solids. Additional heteroatom oligomers were also recently identified in

87 thermally aged $GaAl_{12}$ and $GeAl_{12}$ bearing solutions and resulted in the isolation of several novel

88 species ($\delta\text{-GaAl}_{12}$, Ga_2Al_{18}, $Ga_{2.5}Al_{28.5}$, Ge_4Al_{48}, $\delta\text{-Cr}_nAl_{13-n}$).[21-24] These heteroatomic clusters

89 have similarities to the $\delta\text{-Al}_{13}$ and Al_{30} phase observed in some PACl coagulants, but have not

90 been evaluated for enhanced coagulation performance. Aggregation behavior is also an important

91 piece that contributes to higher performance of coagulants and controls shelf-life for these

92 commercial products, but a detailed understanding of these processes is lacking within heteroatom

93 Al-Keggin systems.

94   In the current study, we evaluate solutions of as-synthesized MAl_{12} (M= Al, Ga and Ge)

95 clusters that are analogous to commercial coagulate agents. We have hydrothermally aged these

96 solutions for 0 to 7 days to explore their overall aggregation behavior as it relates to formation of

97 oligomeric Keggin-type species. We then evaluated initial assessment of their water treatment

98 efficiency through the comparison of DOC and turbidity removal capacity of different MAl_{12}

99 solutions between a pH range 5-9 using humic acid and kaolin spiked Iowa river water. The result

100 of heteroatom substitution on stability and particle size distribution of aged Keggin solution were

101 evaluated using pH, turbidity, and Dynamic Light Scattering (DLS) measurements. The solid

102 precipitates formed during hydrothermal aging of Keggin solutions were characterized using

103 Powder X-ray diffraction (PXRD), Thermogravimetric Analysis (TGA) and Scanning Electron

104 Microscopy-Energy Dispersive X-ray Spectroscopy (SEM-EDS).

105

106 **Experimental**

107   All chemicals used for experiments ((AlCl$_3$·6H$_2$O (Fisher Scientific), NaOH (Fisher

108 Scientific), anhydrous GaCl$_3$ (Strem Chemicals), GeO$_2$ (Beantown Chemicals), Humic Acid

109 (Sigma-Aldrich) and Kaolin (Beantown Chemicals)) were used as received. Solution utilized in

110 this study were prepared using ultrapure water (18.2 MΩ.cm, Easypure II) as the solvent.

111

112 *Preparing and characterizing MAl$_{12}$ solutions*

113   The Al$_{13}$ stock solution was prepared by following Johansson *et al.*[25] This is the same

114 protocol that is used typically in preparing Keggin-type polyaluminum coagulants (PACl-Al$_{13}$ and

115 PACl-Al$_{30}$).[12, 26] In a typical synthesis, 35 mL of a 0.25M AlCl$_3$ solution was stirred and heated in

116 a 250 mL glass Erlenmeyer flask on water bath until the temperature was stabilized at 80 °C. Upon

117 thermal equilibration of the solution, 84 mL NaOH (0.25M) was added dropwise under constant

118 stirring. The solution was then cooled to room temperature for use in additional experiments.

119   A GaAl$_{12}$ solution was prepared by following procedure of Parker *et al.*[19] with further

120 modification by Shohel *et al.*[21] The stock solution of containing mixed Al^{3+} and Ga^{3+} cations in a

121 6:1 molar ration was formed by combining 30 mL of AlCl$_3$ (0.25 M) and 5 mL of GaCl$_3$ (0.25M)

122 in a 250 mL glass Erlenmeyer flask. This solution was heated in a water bath to 80 °C and partial

123 hydrolysis of the heteroatom solution occurred through the addition of 84 mL of NaOH (0.25 M)

124 in a dropwise fashion under constant stirring.

Similarly, the $GeAl_{12}$ stock solution prepared by following Lee *et al.*[20] with further modification adopted from Shohel et al.[23] Initially a Ge^{4+} stock solution was prepared by adding 0.088 g GeO_2 to 96 mL of NaOH (0.25 M) with constant stirring for 20 minutes. This solution was then utilized to partially hydrolyze 40 mL of 0.25M $AlCl_3$ under constant stirring at 80 ^{o}C.

Thermal aging of the stock solutions occurred by loading 15 ml of the prepared MAl_{12} (M = Al^{3+}, Ga^{3+}, and Ge^{4+}) stock solutions into individual 125 mL Teflon-lined Parr vessels and heated in a gravimetric oven set at 90 ^{o}C. As-prepared/unaged solutions are designated as 0 day and then additional hydrothermal aging was completed for 1, 3, and 7 days.

Solution pH and turbidity of all aged and unaged MAl_{12} samples were measured using a VWR SB70P pH probe and Hach 2100N turbidity meter, respectively. Hydrodynamic diameter of MAl_{12} species in solution was analyzed by Malvern Zetasizer NanoZS. Both Al_{13} and $GaAl_{12}$ solutions were filtered through a 0.45 µm membrane filter prior to DLS measurement to analyze the suspended solids. For $GeAl_{12}$, an extra filtration step with a 0.25 µm membrane filter was necessary due to presence of large amount of solid precipitate that formed in this system. During DLS measurement, at least 20 individuals scan were performed to determine particles size distribution within each solution.

Precipitates were separated from the 7-14 days aged MAl_{12} solution by centrifugation and washed with deionized water. The collected solids were dried in oven at 45 °C for 48 hours and then characterized by quantitative gravimetric analysis, Powder X-Ray Diffraction (PXRD), Scanning Electron Microscopy-Energy Dispersive X-ray Spectroscopy (SEM-EDS) and Thermogravimetric Analysis (TGA). Quantitative gravimetric analysis was performed on precipitates separated from MAl_{12} aged (14 days) solutions with a Metler Toledo AT20 analytical microbalance. PXRD of samples were performed using Bruker D8 Discover Diffractometer

148 equipped with Cu Kα (λ = 1.5406 Å) radiation and multimode EIGER2R detector. Solid samples

149 were deposited on a zero-background silicon wafer and the data was collected from 10-80° 2θ with

150 a step size of 0.2° and a count time of 5 sec/step. Thermal stability and dehydration of the collected

151 solids were determined by placing 5-10 mg into an aluminum pan and heating on a TA instruments

152 Q500 thermogravimetric analyzer (TGA) at a ramp rate of 10 °C/min. Weight loss data was

153 collected from 20 °C to 600 °C using high purity N_2 as the carrier gas. SEM-EDS was used to

154 image and qualitatively assess elemental composition of carbon-coated precipitates. The samples

155 were placed on a Hitachi S-3400N system equipped with silicon drift detector (XFlash, Bruker

156 AXS) and measurements were carried out at 15 kV beam energy with a 2.5 minute exposure time

157 and 10 mm of working distance.

158

159 *Water treatment: DOC removal and Turbidity*

160   Natural water used for water treatment experiments was collected from Iowa river near the

161 University of Iowa campus in February 2020. The physical parameter of collected river water was

162 measured for the overall sample (pH= 7.95, turbidity before settling= 20.0, turbidity after settling

163 24 hours= 3.60, UV-Vis absorption at 254 nm= 0.0656). Water quality parameters for the

164 collection site of Iowa river is provided by the Iowa Department of Natural resources (Supporting

165 Information Table S2). Settled river water was used for water treatment experiments in accordance

166 with previous studies.[15, 27]

167   Humic acid was used to evaluate DOC removal efficiency of aged and unaged MAl_{12}

168 solutions at pH= 5, 6, 7, 8, and 9. A stock solution of humic acid with concentration 1.0 g/L was

169 prepared in water and filtered with Whatman® filter paper (Grade: 1, diameter: 100 mm, pore size:

170 11 µm). Following filtration, 21mL of the stock humic acid solution was then homogeneously

171 mixed with 140 mL of river water. The pH of the Humic Acid spiked River Water (HARW) was

172 then adjusted into desired value using few drops of 1 M or 0.25 M aqueous HCl and NaOH. The

173 absorption spectra of the HARW solution was collected in quartz cuvette on a Cary 5000 UV

174 spectrometer (Agilent technology). The 254 nm wavelength was used to evaluate DOC content.[28]

175 This pH adjusted HARW sample before flocculation experiments had measurable absorption

176 values ~0.80 at 254 nm in the UV/Vis spectrum. For the DOC removal experiments, 10 mL of the

177 HARW solution was placed into separate 20.0 mL glass scintillation vials, followed by addition

178 of 25 µL of the prepared MAl_{12} solutions. These solutions were then stirred for 25 minutes with a

179 magnetic stir bar (15.9 x 8 mm) at 200 rpm for the overall flocculation reaction. The generated

180 flocs were initially separated by centrifugation at 6000 rpm, followed by a secondary filtration

181 using 0.45 µm membrane filter. The absorption spectra of treated water and HARW solution was

182 collected and the % DOC removal for all samples as outlined by Weishaar *et al.*[28]

183   To evaluate turbidity removal, 55 mg of kaolin was added to 660 mL river water in a 1.5

184 L glass jar and shaken vigorously for five minutes. The pH of the solution was then adjusted to the

185 desired value using 1 M or 0.25 M aqueous HCl and NaOH. Turbidity of stock solution was

186 initially measured using a Hach 2100N turbidity meter to be 90 nephelometric turbidity units

187 (NTU). The impact of the polyaluminum clusters on solution turbidity was evaluated by adding

188 1.0 mL of each MAl_{12} solution into a separate 50 mL aliquot of the prepared kaolin spiked river

189 water in a 60 mL transparent reagent bottle with a magnetic stir bar (15.9 x 8 mm). This solution

190 was initially mixed for one minute at 400 rpm and then stirred for an additional 10 minutes at 100

191 rpm. Generated flocs were then allowed to separate via gravitational settling over the course of

192 40 minutes before 30 mL of the solution was carefully removed from bottle using a pipette. The

193 solution from the top 0.5 cm and bottom 2.0 cm were not sampled so that the solution represented

194 the residual turbidity measurement. These solutions were again analyzed using a Hach 2100N
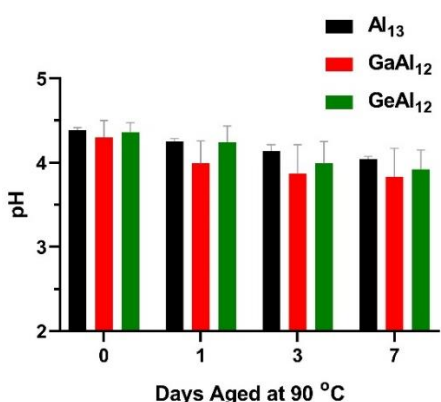
195 turbidity meter.

196

197 **Result and Discussion**

198

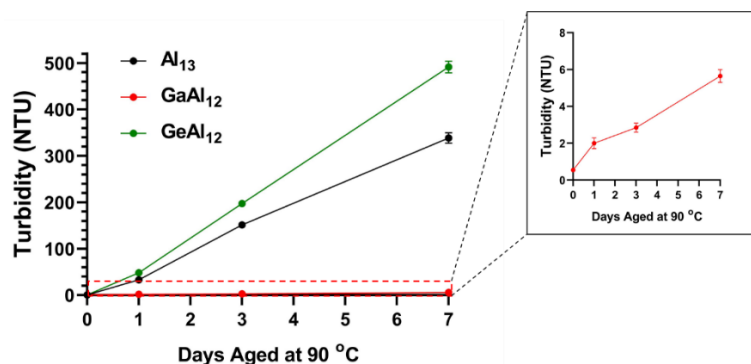199 *Characterization of MAl_{12} solutions*

200 　　　MAl_{12} solutions remained within in a relatively narrow pH range (3.50-4.47), but decreased

201 slightly with hydrothermal aging due to the extended hydrolysis reaction of polyaluminum species

202 **(Figure 1A)**. Continued hydrolysis brought about by aging of the solution leads to the release of

203 H^+ from deprotonation of surface water groups and formation of bridging hydroxyl groups.

204 Previous work by Casey and coworkers demonstrated that the acidity of the ligated water

205 molecules varies as a function of the heteroatom substitution with $GaAl_{12}<Al_{13}<GeAl_{12}$ and this

206 was confirmed with computational results by Bjorklund *et al.*[29, 30] The largest pH differences for

207 all three samples were observed between 0 to 1 day (2.75 – 7.20 %) and then from 1 to 3 days

208 (2.59 - 5.89 %). The smallest difference in the solution pH was observed between 3 to 7 days (1.03

209 – 2.41 %), suggesting that the forward reaction for the oligomerization process was likely nearing

210 equilibrium.

211 　　　Turbidity of MAl_{12} solutions during hydrothermal aging varied significantly, with visible

212 differences observed for the heteroatom substitution. All initial MAl_{12} solutions were visibly clear

213 with no observable precipitate at the bottom of the vial prior to the aging process. This was also

214 confirmed by turbidity measurements with values of 0.50- 0.85 NTU. Upon hydrothermal aging,

215 increased turbidity was noted for the Al_{13} and $GeAl_{12}$ solutions, whereas the $GaAl_{12}$ aged solutions

216 visibly remained clear (**Figure 1C**). The NTU values for the MAl_{12} solutions reveals that the
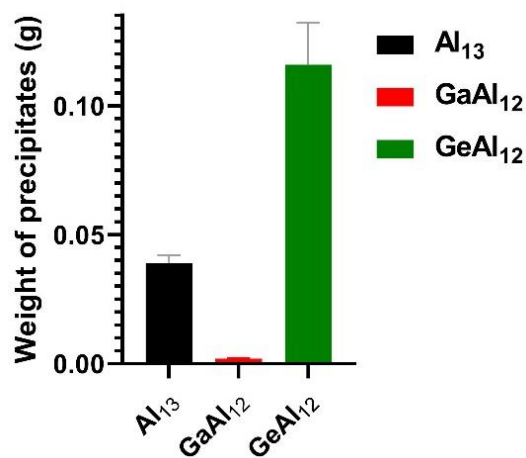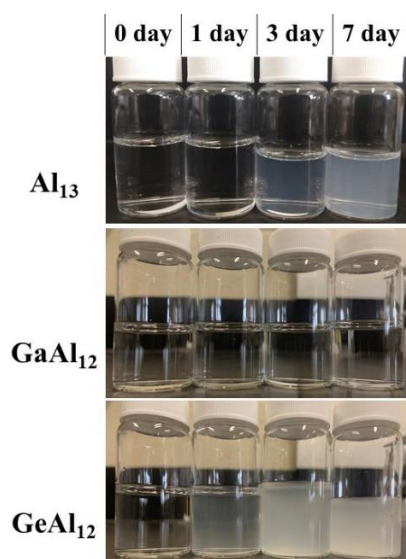
217   GeAl$_{12}$ solutions are more turbid than Al$_{13}$ at the same time points (**Figure 1B**). We have also

218   noted that although GaAl$_{12}$ aged solutions are visibly transparent, turbidity measurements

219   indicated a small increase with aging time (2.00- 5.65 NTU). Colloidal particles for all MAl$_{12}$

220   solutions aggregated at the bottom of the vial if left undisturbed for two days. The gravimetric

221   analysis of precipitates formed after 14 days of aging have also shown formation of more insoluble

222   matter for GeAl$_{12}$ solution with quantified mass of 115.85 ± 16.85 mg (**Figure 1D**). Whereas,

223   GaAl$_{12}$ solution formed only 2 ± 0.02 mg precipitates and 39.1 ± 2.9 mg were recovered from the

224   Al$_{13}$ solution.

(A)

(B)

10

(C)   **(D)**

Figure 1. The **(A)** pH, **(B)** turbidity, **(C)** physical appearance and **(D)** mass of precipitates recovered from MAl_{12} solutions during hydrothermal aging at 90 °C.

225   Dynamic light scattering (DLS) measurements were also utilized to analyze the particle

226   size in filtered MAl_{12} solutions and probe formation of polyaluminum species. It is important to

227   note that colloidal species scatter with higher intensity than smaller polyaluminum species is

228   solution;[31, 32] thus, we utilize this technique to compare differences in particle size distribution

229   between the pure Al_{13} and Ge^{4+}- or Ga^{3+}-substituted version and not relative amounts of the

230   particles in the solution. For unaged Al_{13} solution there are two peaks, with the feature at 1.5 nm

231   corresponding to the hydrodynamic diameter of the Al_{13} Keggin-type species and a second one at

232   >100 nm that belongs to $Al(OH)_3$ colloids. Upon aging, the peak at 1.5 nm disappeared and only

233   the colloidal species (>100 nm) remained in solution. For unaged $GaAl_{12}$ solution, we have

234   observed multiple peaks in <100 nm range with center at hydrodynamic diameter 1.5, 8, and 72

235   nm. After one and three days of aging, the peak at 1.5 nm remained in the size plot, but the second

236   peak shifted to 11.7 nm. The 1.5 nm peak was not present after 7 days of aging $GaAl_{12}$ solution,

237   but peaks at 11.7 nm and 60 nm were present in the size plot. For $GeAl_{12}$, the unaged solution has

238   two features in the <100 nm region: one centered at 1.3 nm and a second, broad peak at

239   approximately 15 nm. After thermal aging the $GeAl_{12}$ solution, a feature at 2.8 nm on day 3 appears

240   and becomes more intense after 7 days of treatment.

241   Based upon our current understanding of the known Al^{3+} polycation species, we can

242   tentatively assign the peaks observed in the DLS. The peak in unaged Al_{13} and $GaAl_{12}$ solution at

243   approximately 1.5 nm aligns well with the expected hydrodynamic diameter for the known

244   polyaluminum species Al_{13}, Al_{30}, $GaAl_{12}$ or $Ga_{2.5}Al_{28.5}$ species in solution.[21, 33-35] Features at 8 nm

245   and 15 nm for unaged $GaAl_{12}$ and $GeAl_{12}$ solution may correspond to the aggregation of smaller

246   clusters. For the $GeAl_{12}$ solutions, the peak at 1.3 nm can be correlated to a $GeAl_{12}$ species and the

247   feature at 2.8 nm have been reported due to the formation of the Ge_4Al_{48} species from condensation

248   of $GeAl_{12}$.[23] In addition, all three systems contain particles with sizes greater than 10 nm that

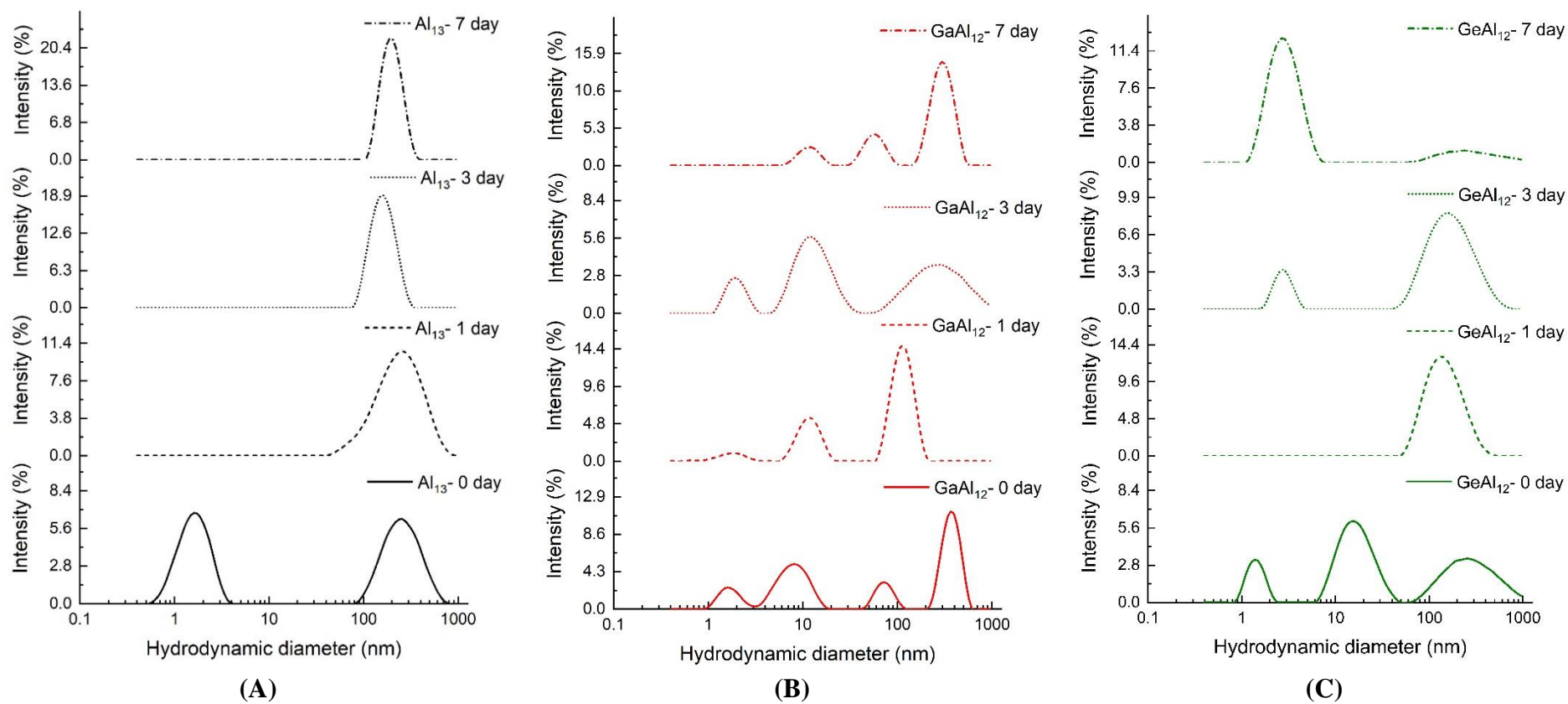249   contribute to the turbidity of the system and are likely associated with aggregated Keggin-type

250   particles.

251

252

253

254

255

256

257

Figure 2. Particle size distribution from DLS measurement in aged and unaged solution of **(A)** Al_{13}, **(B)** $GaAl_{12}$ and **(C)** $GeAl_{12}$.

258

259 *Characterization of precipitates formed from the MAl$_{12}$ system.*

260   Changes in turbidity within the Al^{3+} system is caused by nucleation and precipitation of

261 solid hydroxide phases. To further explore the solid precipitate, we performed additional chemical

262 characterization of the insoluble flocculant to provide a deeper insight into the structure and

263 composition. The PXRD of all precipitates contain a broad feature below 15° 2θ value, suggesting

264 formation of an amorphous material (**Figure S1**). There are small sharp peaks located at 27.38,

265 31.72, 45.46, and 56.48° 2θ value for all precipitates due to the presence of NaCl salts that

266 crystalize during sample drying. Morphological analysis of the particles observed with SEM

267 suggest the presence of both micron and submicron particles in all precipitates (**Figure S2**). EDS

268 analysis identifies the presence of Al, O, Na and Cl in the precipitate obtained from Al$_{13}$ solution

269 (**Table S1**), corroborating our PXRD analysis. EDS also indicated that Ga and Ge were both

270 associated with precipitates collected from GaAl$_{12}$ and GeAl$_{12}$ solutions, respectively. Given the

271 incorporation of Ga and Ge into the Keggin-type topology, we hypothesized that similar ratios

272 would be observed within the amorphous material. Based upon the semi-quantitative amounts

273 obtained from the SEM-EDS, we can say that the Ga^{3+} and Ge^{4+} contents are enriched (Al:Ga ratio

274 = 12:3.8 and Al:Ge ratio = 12:2 with Al:M = 12:1 for MAl$_{12}$ Keggin) in the precipitate.

275   We have also observed difference in TGA patterns among precipitates collected from

276 different MAl$_{12}$ solutions. All the precipitates continuously lost 27.9-33.6% weight as the

277 temperature increased from 20 to 600 °C (**Figure 3A and 3B**). The derivative weight loss indicates

278 that the precipitates have two observable two weight loss steps, with the first occurring between

279 30-150 °C for a total decrease of 6.9, 12.1, and 10.3 wt. % for Al$_{13}$, GeAl$_{12}$, and GaAl$_{12}$,

280 respectively. The second weight loss for these samples occur between 230-520 °C for both Al$_{13}$

281 and $GeAl_{12}$ precipitates with a decrease of 14.3% and 13.9%, respectively. This second step occurs

282 over a lower temperature range (185 - 360 °C) for the $GaAl_{12}$ system with weight loss 10.0% .
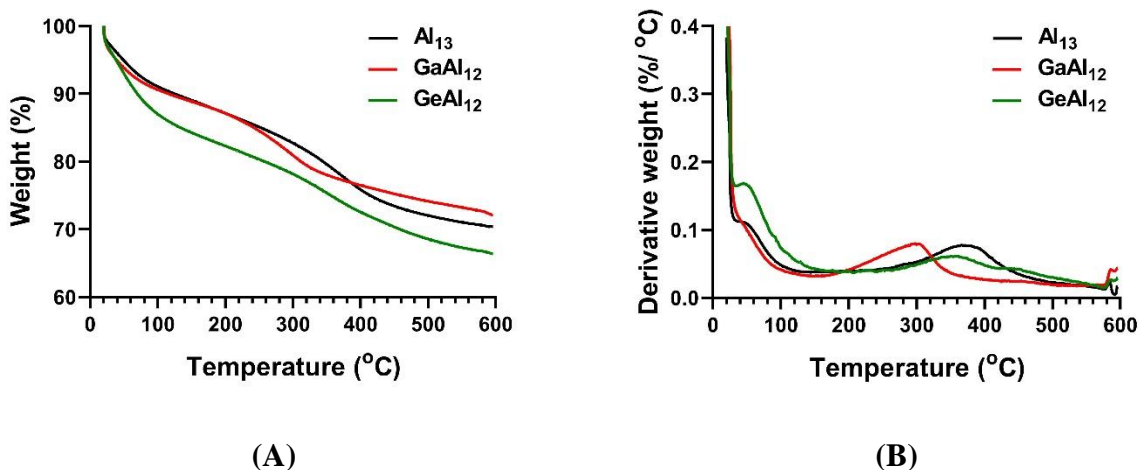
283

(A)   **(B)**

284 **Figure 3.** (**A**) Thermogravimetric pattern and (**B**) Derivative thermogravimetric (DGT) plot of

285 precipitate formed during thermal aging of MAl_{12} solution.

286   Similar TGA results have also been reported for the Al^{3+} system. Two weight loss steps

287 have been reported earlier for different $Al(OH)_3$ phases, with first one occurring between 30-140°C

288 and corresponding to removal of surface adsorbed water, and the second weight loss (>200°C)

289 correspond to removal of hydroxyl groups to form Al_2O_3.[36, 37] The second weight loss steps varied

290 for different $Al(OH)_3$ phases and their synthesis condition. Sato reported that the second weight

291 loss occurred between 290-350°C for amorphous $Al(OH)_3$, 400-500°C for pseudoboehmite

292 ((AlO(OH)), 220-350 °C for bayerite (α-$Al(OH)_3$), and 360-520°C for boehmite((γ-AlO(OH)).[36]

293 For gibbsite (γ-$Al(OH)_3$), the removal of the hydroxyl groups occurred in two steps: between 260-

294 330 °C and 460-540 °C.[37] Within our system, it seems that Al_{13} and $GeAl_{13}$ transition occur in the

295 region more aligned with boehmite or pseudoboehmite phases and the $GaAl_{12}$ system transition

296 occurs closer to the transition for amorphous $Al(OH)_3$ or bayerite. Interestingly, the general order

297   of solubility at room temperature is gibbsite < boehmite < bayerite, which aligns with the relative

298   amount of precipitate that was formed from the MAl_{12} system[38].

299   Our TGA results align well with previously literature results regarding the precipitation of

300   solid phases from the Al_{13} Keggin system. During aging, the original ε-Al_{13} phase can first

301   transform into soluble oligomeric species (e.g. Al_{26}, Al_{30}) and then form insoluble $Al(OH)_3$

302   precipitates.[39, 40] The exact nature of the solid precipitate that is formed from this process is

303   dependent on the exact solution conditions. When an unhydrolyzed Al^{3+} solution is aged at higher

304   temperature (which likely results in the formation of Keggin species, the precipitate that forms is

305   believed to be poorly crystalline pseudoboehmite $(AlO(OH))$.[5] Similarly alumina sol-gels that

306   contain Al_{13} Keggin species have also been shown to create a pseudoboehmite solid phase upon

307   aging[5]. Hsu evaluated the room temperature aging of Al_{13} solution created through the addition

308   of carbonate as the hydrolyzing agent and observed that the resulting precipitation in this case was

309   crystalline gibbsite $(Al(OH)_3)$.[40] For this system the author suggested that the mechanism of

310   gibbsite formation began with the breakdown of the Al_{13} polycations into monomeric specie,

311   which could then rearrange to form the gibbsite structure. Non-classical mechanisms that results

312   from structural transformation of the oligomeric phases may also be at play in the transition of an

313   amorphous flocculant into a crystalline phase.[41-45]

314   With the inclusion of the heteroatom, we do see differences in the second weight loss

315   step that may suggest subtle differences in the resulting phase and this is supported by previous

316   studies within Fe^{3+} systems. Similar to Al^{3+} chemistry, Fe^{3+} also undergoes hydrolysis reaction in

317   aqueous systems and will rapidly precipitate amorphous or poorly crystalline nanoparticulate

318   phases that can contain a significant fraction of non-stoichiometric dopants[46, 47]. If we look

319   specifically at Al^{3+} as the dopant, previous studies have shown that Fe^{3+} will readily form a solid-

320 solution series with an upper limit of 30% Al^{3+} substitution[46, 48-50]. Phase transformations for these

321 Al^{3+} doped materials vary depending on the presence of the heteroatom in the system. For instance,

322 Al^{3+} doped ferrihydrite will favor the formation of hematite over goethite. Adding Al^{3+} to goethite

323 will also cause a systematic shift in the temperature region associated with the removal of hydroxyl

324 groups, which is similar to the region that is associated with the $GaAl_{12}$ and $GeAl_{12}$ systems[47]. The

325 transformational changes observed with Al^{3+} doping within Fe^{3+} mineral phases suggest that we

326 should expect similar variability to occur within the $GaAl_{12}$ and $GeAl_{12}$ systems and supports our

327 current TGA results.0

328 *Water treatment: Removal of DOC and Turbidity from Iowa River Water Samples*

329 Removal efficiency of DOC from aged and unaged MAl_{12} solutions was determined to be

330 pH dependent, where the % removal for all MAl_{12} solutions increase with decreasing pH. This

331 result aligns well with previous work reported by Zhang *et al.* 2008 as they also found that humic

332 acid removal by PACl-Al30 increased as the has the pH of the solutions were lowered from 9 to

333 4[51]. They suggested that the labile protons on the surface of the Keggin species in the coagulant

334 enables significant charge-neutralization of the humic acid, which destabilizes the macromolecule

335 and allows flocculation to occur. Additionally, the stability of the Keggin species in solution is

336 optimal at a pH of 4-5; thus, higher pH values may have competition between charge neutralization

337 of the DOC and continued metal hydrolysis of the soluble clusters.

338 Subtle differences are observed in % DOC removal that can be related to the heteroatom

339 substitution and aging time. For unaged solution, $GaAl_{12}$ performed slightly better in higher pH

340 (7-9), followed by Al_{13} and $GeAl_{12}$. At pH 5 and 6, unaged $GeAl_{12}$ had the highest % DOC removal

341 followed by Al_{13} and $GeAl_{12}$. Aging time increases the % DOC removal for Al_{13} and $GaAl_{12}$, with

342 an exception of Al_{13} solution at pH 9 where we observe a decrease. The $GeAl_{12}$ solutions display

343 a different trend, with an initial increase in % removal after one day aging, followed by a

17

344 systematic decrease for 3 and 7 day aging. We note that the $GeAl_{12}$ solutions also displayed the

345 greatest amount of precipitant formed upon aging, so this may also account for the decrease in the

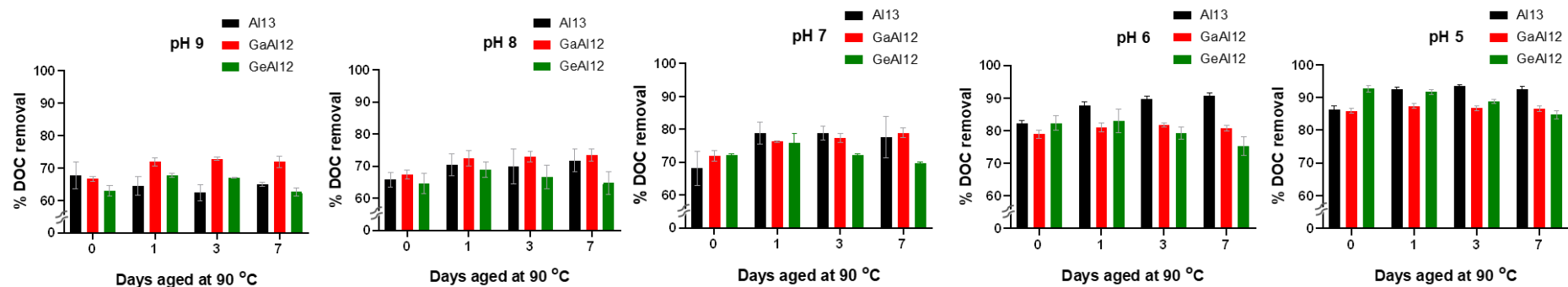346 overall efficiency observed in this system.

347

Figure 4. DOC removal efficiency of unaged and aged MAl_{12} solutions from humic acid spiked Iowa river water at different pH.

352   Trends related to the turbidity removal efficiency for kaolin spiked Iowa river water using

353   the MAl_{12} solutions are less clear than those observed for % DOC. The turbidity removal

354   efficiency of most solutions was lower when the pH was decreased from 9 to 7, but the turbidity

355   removal from pH 7 to 5 does not follow a clear pattern. For example, a turbidity removal efficiency

356   increased between a pH 7 to 6, but decreased when we moved from pH 6 to 5. In general, 1 to 3

357   days aging increased the turbidity removal efficiency of MAl_{12} solutions at different pH, but 7

358   days aging most cases decreases the efficiency. When comparing effect of heteroatom substitution

359   in unaged solution, Al_{13} or $GeAl_{12}$ demonstrated better turbidity removal compared to $GaAl_{12}$ at

360   higher pH (9 to 8). But at lower pH (7 to 5), the turbidity removal efficiency trends were $GaAl_{12}$

361    $>GeAl_{12}>Al_{13}$. For aged solution, $GaAl_{12}$ showed superior performance followed by $GeAl_{12}$ and

362   Al_{13} at most pH ranges. Interestingly pH 9 was the exception because the $GeAl_{12}$ solution

363   demonstrated higher efficiency in turbidity removal. The aged $GaAl_{12}$ solutions consistently

364   removed turbidity at all pH ranges and this is specifically apparent at pH 5, where the aged $GaAl_{12}$

365   solutions showed remarkably high turbidity removal performance compared to other solutions.
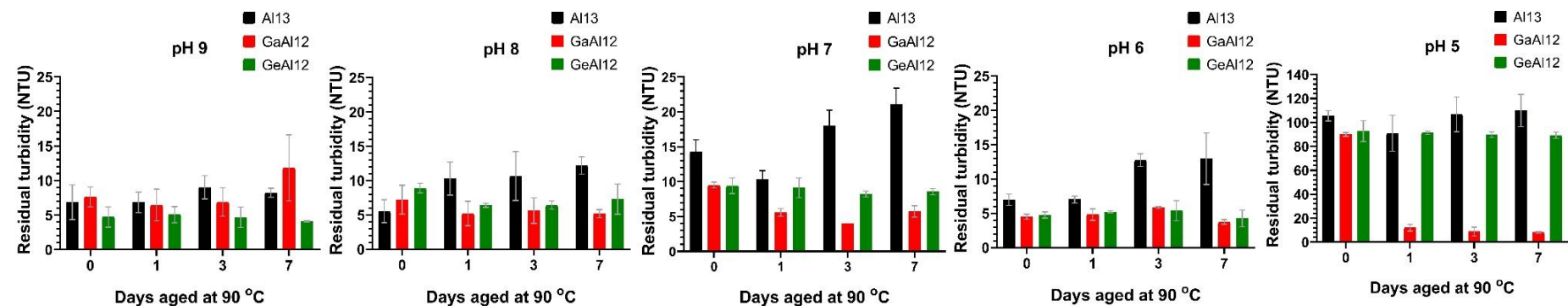
Figure 5. Turbidity removal efficiency of unaged and aged MAl$_{12}$ solutions through residual turbidity measurement of kaolin spiked Iowa river water at different pH.

371   Our results suggesting that heteroatom substitutions in Al_{13} and subsequent hydrothermal

372   aging have significant impact in their water treatment efficiency with respect to DOC and turbidity

373   removal. We have observed that although at higher pH the water treatment efficiency of $GaAl_{12}$ is

374   better than Al_{13} and $GeAl_{12}$, this trend does not hold true for lower pH values for DOC removal.

375   Turbidity removal of the $GaAl_{12}$ aged and unaged solutions display superior capability in all pH

376   range (9-5) compared to other MAl_{12} solutions, with the highest performance observed at pH 5.

377   Previous work by Stewart et al. 2009, indicated that the $GaAl_{12}$ stock solution performed

378   better in water treatment due to its relative stability, lower acidity, and tendency not to form larger

379   clusters and oligomers.[15] The turbidity and gravimetric experiment from our study also showed

380   relative stability of $GaAl_{12}$ with respect to the transformation of polyaluminum species into

381     $Al(OH)_3$ based precipitate. Our DLS experiment also showed similar particle size distribution for

382   polyaluminum species in unaged to 3 days aged $GaAl_{12}$ solution which maybe an indication of

383   stability and less oligomerization behavior. When the article by Stewart et al. was published in

384   2009, there was no experimental evidence that larger oligomers with the $GaAl_{12}$ system existed,

385   but more recent efforts suggested that $Ga_{2.5}Al_{28.5}$ and Ga_2Al_{18} do occur in aged solutions.[15] These

386   newer species having different charge, size and surface characteristic than the ε-Keggin and may

387   have better capability to neutralize the contaminant and without destabilizing the clusters from

388   solution. For example, solutions containing Al_{30} polyaluminum clusters demonstrated higher floc

389   formation capacity than Al_{13} bearing solutions and this was linked to a higher number of adsorption

390   sites, more neutralization capacity, and better solution stability (temperature and pH).[12] Owing to

391   those physicochemical changes, Al_{30} is a better turbidity removal agent at wider pH range then

392   Al_{13}. This suggests that the presence of $Ga_{2.5}Al_{28.5}$ and Ga_2Al_{18} could also enhance the removal of

393   DOC and turbidity from natural water samples.

Conclusion

In conclusion, our study demonstrated that heteroatom substitution in ε-Al_{13} have profound impact on their transformation into other polyaluminum species and insoluble hydroxides. Overall, the $GaAl_{12}$ solution was more stable during thermal aging than Al_{13} or $GeAl_{12}$ and DLS results indicated that this system possessed more diversity within the soluble particle size. In addition, the resulting precipitant form the aging study for $GaAl_{12}$ was found to behave in a similar manner upon heating and may contain structural features with similarities to amorphous $Al(OH)_3$ or bayerite phase, which is known to have higher solubility than other Al^{3+} phases. This chemical transformation governs the stability of soluble species and their coagulation performance, including the formation of larger oligomers that may increase % DOC and turbidity removal.

Results from present work will shed new light on the development of highly effective aluminum-oxo Keggin polycation based coagulants. The difference in water treatment efficiency of different heteroatom-substituted and aged Keggin solution pointing towards importance of further investigations to identify the different possible oligomers that may be present in the system. Overall, the relatively coagulation efficiency may depend on a smaller number of more reactive species to achieve the systems level observables that are measured during experimental evaluation of flocculation behavior and contaminant removal. Continued advancements in understanding of the fundamental changes to surface chemistry and stability of both pure and doped Keggin-type polyaluminum coagulants can lead to a targeted approached toward water purification efforts.

Associated Content

415   The Supporting Information file for this draft is available. The supporting information file

416   contains additional images and results of turbidity measurement, PXRD analysis and SEM-EDS

417   analysis.

418

419   **Author Contributions**

420   MS conceived the study, designed experiments, did all chemical analysis, led water

421   treatment experiments, and prepared initial draft of the study. JAS prepared MAl_{12} solutions,

422   performed water treatment experiments and contributed in writing initial draft. MAC helped with

423   turbidity experiment. TZF provided resources, guided conceptualization of the study, ensured

424   method validation, and edited the manuscript. All author contributed in preparation and revision

425   of the manuscript.

426

427   **Notes**

428   The authors declare no conflict of interest.

429

430   **Acknowledgement**

431   We acknowledge Prof. Aliasger Salem and Dr. Lr Jaidev Chakka (UIowa college of

432   Pharmacy) for their help regarding DLS experiment. We also acknowledge help of Phil Pagano

433   (Center for Research, Exploration, and Advanced Technology in Engineering and Sciences, Iowa

434   CREATES) for his help with SEM-EDS analysis. We thank Prof. Craig L. Just (UIowa, Civil and

435   Environmental Engineering) to let us use the turbidity meter.

436
437   **References**

438

439   1.   EPA National Pollutant Discharge Elimination System Permit Writer's Manual: Chapter 5

440   Technology-Based Effluent Limitations https://www.epa.gov/npdes/npdes-permit-writers-manual

441   (accessed 10/06/2020).

442   2.   *Standard methods: for the examination of water and wastewater*. American Public Health

443   Association: Washington, D.C, 1989; p 10200.

444   3.   Casey, W. H., Large Aqueous Aluminum Hydroxide Molecules. *Chem. Rev.* **2006,** *106* (1), 1-16.

445   4.   Abeysinghe, S.; Unruh, D. K.; Forbes, T. Z., Crystallization of Keggin-Type Polyaluminum Species

446   by Supramolecular Interactions with Disulfonate Anions. *Crystal Growth & Design* **2012,** *12* (4), 2044-

447   2051.

448   5.   Fu, G.; Nazar, L. F.; Bain, A. D., Aging processes of alumina sol-gels: characterization of new

449   aluminum polyoxycations by aluminum-27 NMR spectroscopy. *Chem. Mater.* **1991,** *3* (4), 602-610.

450   6.   Furrer, G.; Phillips, B. L.; Ulrich, K.-U.; Pöthig, R.; Casey, W. H., The Origin of Aluminum Flocs in

451   Polluted Streams. *Science* **2002,** *297* (5590), 2245.

452   7.   Sahu, O.; Chaudhari, P., Review on Chemical treatment of Industrial Waste Water. *Journal of*

453   *Applied Sciences and Environmental Management* **2013,** *17* (2), 241-257.

454   8.   Sinha, S.; Yoon, Y.; Amy, G.; Yoon, J., Determining the effectiveness of conventional and

455   alternative coagulants through effective characterization schemes. *Chemosphere* **2004,** *57* (9), 1115-

456   1122.

457   9.   *MWH's water treatment: principles and design*. 3rd ed ed.; John Wiley & Sons: Hoboken, N.J,

458   2012; p 1901.

459   10.   Kweinor Tetteh, E.; Rathilal, S., Application of Organic Coagulants in Water and Wastewater

460   Treatment. In *Organic Polymers*, Sand, A.; Zaki, E., Eds. IntechOpen: 2020.

461   11.   Mertens, J.; Casentini, B.; Masion, A.; Pöthig, R.; Wehrli, B.; Furrer, G., Polyaluminum chloride

462   with high Al30 content as removal agent for arsenic-contaminated well water. *Water Res.* **2012,** *46* (1),

463   53-62.

464   12.   Chen, Z.; Fan, B.; Peng, X.; Zhang, Z.; Fan, J.; Luan, Z., Evaluation of Al30 polynuclear species in

465   polyaluminum solutions as coagulant for water treatment. *Chemosphere* **2006,** *64* (6), 912-918.

466   13.   Yan, M.; Wang, D.; Qu, J.; He, W.; Chow, C. W. K., Relative importance of hydrolyzed Al(III)

467   species (Ala, Alb, and Alc) during coagulation with polyaluminum chloride: A case study with the typical

468   micro-polluted source waters. *J. Colloid Interface Sci.* **2007,** *316* (2), 482-489.

469   14.   Matsui, Y.; Matsushita, T.; Sakuma, S.; Gojo, T.; Mamiya, T.; Suzuoki, H.; Inoue, T., Virus

470   Inactivation in Aluminum and Polyaluminum Coagulation. *Environmental Science & Technology* **2003,** *37*

471   (22), 5175-5180.

472   15.   Stewart, T. A.; Trudell, D. E.; Alam, T. M.; Ohlin, C. A.; Lawler, C.; Casey, W. H.; Jett, S.;

473   Nyman, M., Enhanced Water Purification: A Single Atom Makes a Difference. *Environmental Science &*

474   *Technology* **2009,** *43* (14), 5416-5422.

475   16.   Wu, Z.; Zhang, X.; Pang, J.; Zhang, X.; Li, J.; Li, J.; Zhang, P., Humic Acid Removal from Water

476   with PAC-Al30: Effect of Calcium and Kaolin and the Action Mechanisms. *ACS Omega* **2020,** *5* (27),

477   16413-16420.

478   17.   Demissie, H.; An, G.; Jiao, R.; Ritigala, T.; Lu, S.; Wang, D., Modification of high content

479   nanocluster-based coagulation for rapid removal of dye from water and the mechanism. *Sep. Purif.*

480   *Technol.* **2021,** *259*, 117845.

481   18.   Lu, S.; Liu, L.; Yang, Q.; Demissie, H.; Jiao, R.; An, G.; Wang, D., Removal characteristics and

482   mechanism of microplastics and tetracycline composite pollutants by coagulation process. *Sci. Total*

483   *Environ.* **2021,** *786*, 147508.

484   19.   Parker, W. O. N.; Millini, R.; Kiricsi, I., Metal Substitution in Keggin-Type Tridecameric

485   Aluminum–Oxo–Hydroxy Clusters. *Inorg. Chem.* **1997,** *36* (4), 571-575.

486   20.   Lee, A. P.; Phillips, B. L.; Olmstead, M. M.; Casey, W. H., Synthesis and Characterization of the
487   GeO4Al12(OH)24(OH2)128+ Polyoxocation. *Inorg. Chem.* **2001,** *40* (17), 4485-4487.

488   21.   Shohel, M.; Bjorklund, J. L.; Ovrom, E. A.; Mason, S. E.; Forbes, T. Z., Ga3+ Incorporation into
489   Al13 Keggin Polyoxometalates and the Formation of δ-(GaAl12)7+ and (Ga2.5Al28.5)19+ Polycations.
490   *Inorg. Chem.* **2020,** *59* (15), 10461-10472.

491   22.   Fairley, M.; Corum, K. W.; Johns, A.; Unruh, D. K.; Basile, M.; de Groot, J.; Mason, S. E.;
492   Forbes, T. Z., Isolation and characterization of the [Ga2Al18O8(OH)36(H2O)12]8+ cluster: cationic
493   variations on the Wells–Dawson topology. *Chem. Commun.* **2015,** *51* (62), 12467-12469.

494   23.   Shohel, M.; Bjorklund, J. L.; Smith, J. A.; Kravchuk, D. V.; Mason, S. E.; Forbes, T. Z., Formation
495   of Nanoscale [Ge4O16Al48(OH)108(H2O)24]20+ from Condensation of ε-GeAl128+ Keggin Polycations.
496   *Angew. Chem. Int. Ed.* **2021,** *60* (16), 8755-8759.

497   24.   Bjorklund, J. L.; Shohel, M.; Bennett, J. W.; Smith, J. A.; Carolan, M. E.; Hollar, E.; Forbes, T. Z.;
498   Mason, S. E., Density functional theory and thermodynamics analysis of MAl12 Keggin substitution
499   reactions: Insights into ion incorporation and experimental confirmation. *The Journal of Chemical*
500   *Physics* **2021,** *154* (6), 064303.

501   25.   Johansson, G.; Dorm, E.; Seleborg, M.; Motzfeldt, K.; Theander, O.; Flood, H., The Crystal
502   Structures of [Al2(OH)2(H2O)8](SO4)2.2H2O and [Al2(OH)2(H2O)8](SeO4)2.2H2O. *Acta chemica*
503   *Scandinavica.* **1962,** *16*, 403-420.

504   26.   Lin, J.-L.; Huang, C.; Chin, C.-J. M.; Pan, J. R., The origin of Al(OH)3-rich and Al13-aggregate flocs
505   composition in PACl coagulation. *Water Res.* **2009,** *43* (17), 4285-4295.

506   27.   Lin, J.-L.; Huang, C.; Pan, J. R.; Wang, D., Effect of Al(III) speciation on coagulation of highly
507   turbid water. *Chemosphere* **2008,** *72* (2), 189-196.

508   28.   Weishaar, J. L.; Aiken, G. R.; Bergamaschi, B. A.; Fram, M. S.; Fujii, R.; Mopper, K., Evaluation of
509   Specific Ultraviolet Absorbance as an Indicator of the Chemical Composition and Reactivity of Dissolved
510   Organic Carbon. *Environmental Science & Technology* **2003,** *37* (20), 4702-4708.

511   29.   Lee, A. P.; Furrer, G.; Casey, W. H., On the Acid–Base Chemistry of the Keggin Polymers: GaAl12
512   and GeAl12. *J. Colloid Interface Sci.* **2002,** *250* (1), 269-270.

513   30.   Bjorklund, J. L.; Bennett, J. W.; Forbes, T. Z.; Mason, S. E., Modeling of MAl12 Keggin
514   Heteroatom Reactivity by Anion Adsorption. *Crystal Growth & Design* **2019,** *19* (5), 2820-2829.

515   31.   Wishard, A.; Gibb, B. C., Dynamic light scattering – an all-purpose guide for the supramolecular
516   chemist. *Supramol. Chem.* **2019,** *31* (9), 608-615.

517   32.   Stetefeld, J.; McKenna, S. A.; Patel, T. R., Dynamic light scattering: a practical guide and
518   applications in biomedical sciences. *Biophysical reviews* **2016,** *8* (4), 409-427.

519   33.   Rowsell, J.; Nazar, L. F., Speciation and Thermal Transformation in Alumina Sols: Structures of
520   the Polyhydroxyoxoaluminum Cluster [Al30O8(OH)56(H2O)26]18+ and Its δ-Keggin Moieté. *J. Am. Chem.*
521   *Soc.* **2000,** *122* (15), 3777-3778.

522   34.   Allouche, L.; Gérardin, C.; Loiseau, T.; Férey, G.; Taulelle, F., Al30: A Giant Aluminum
523   Polycation. *Angew. Chem. Int. Ed.* **2000,** *39* (3), 511-514.

524   35.   Deschaume, O.; Breynaert, E.; Radhakrishnan, S.; Kerkhofs, S.; Haouas, M.; Adam de
525   Beaumais, S.; Manzin, V.; Galey, J.-B.; Ramos-Stanbury, L.; Taulelle, F.; Martens, J. A.; Bartic, C.,
526   Impact of Amino Acids on the Isomerization of the Aluminum Tridecamer Al13. *Inorg. Chem.* **2017,** *56*
527   (20), 12401-12409.

528   36.   Sato, T., The thermal transformation of Gelatinous Aluminium Hydroxide. *Z. Anorg. Allg. Chem.*
529   **1972,** *391* (2), 167-173.

530   37.   Kloprogge, J. T.; Ruan, H. D.; Frost, R. L., Thermal decomposition of bauxite minerals: infrared
531   emission spectroscopy of gibbsite, boehmite and diaspore. *Journal of Materials Science* **2002,** *37* (6),
532   1121-1129.

533 38.   Bénézeth, P.; Hilic, S.; Palmer, D. A., The Solubilities of Gibbsite and Bayerite Below 100 °C in
534 Near Neutral to Basic Solutions. *J. Solution Chem.* **2016,** *45* (9), 1288-1302.
535 39.   Allouche, L.; Taulelle, F., Conversion of Al13 Keggin ε into Al30: a reaction controlled by
536 aluminum monomers. *Inorg. Chem. Commun.* **2003,** *6* (9), 1167-1170.
537 40.   Hsu, P. H., Mechanisms of Gibbsite Crystallization from Partially Neutralized Aluminum Chloride
538 Solutions. *Clays Clay Miner.* **1988,** *36* (1), 25-30.
539 41.   Hou, Y.; Zakharov, L. N.; Nyman, M., Observing Assembly of Complex Inorganic Materials from
540 Polyoxometalate Building Blocks. *J. Am. Chem. Soc.* **2013,** *135* (44), 16651-16657.
541 42.   Demichelis, R.; Raiteri, P.; Gale, J. D.; Quigley, D.; Gebauer, D., Stable prenucleation mineral
542 clusters are liquid-like ionic polymers. *Nature Communications* **2011,** *2* (1), 590.
543 43.   Dey, A.; Bomans, P. H. H.; Müller, F. A.; Will, J.; Frederik, P. M.; de With, G.; Sommerdijk, N. A.
544 J. M., The role of prenucleation clusters in surface-induced calcium phosphate crystallization. *Nature*
545 *Materials* **2010,** *9* (12), 1010-1014.
546 44.   Gebauer, D.; Kellermeier, M.; Gale, J. D.; Bergström, L.; Cölfen, H., Pre-nucleation clusters as
547 solute precursors in crystallisation. *Chem. Soc. Rev.* **2014,** *43* (7), 2348-2371.
548 45.   Yang, X.; Wang, M.; Yang, Y.; Cui, B.; Xu, Z.; Yang, X., Physical origin underlying the
549 prenucleation-cluster-mediated nonclassical nucleation pathways for calcium phosphate. *PCCP* **2019,** *21*
550 (27), 14530-14540.
551 46.   Cornell, R. M.; Schwertmann, U., *The Iron Oxides: Structure, Properties, Reactions, Occurences*
552 *and Uses*. 1 ed.; Wiley: 2003.
553 47.   Pinney, N.; Morgan, D., Thermodynamics of Al-substitution in Fe-oxyhydroxides. *Geochim.*
554 *Cosmochim. Acta* **2013,** *120*, 514-530.
555 48.   Lewis, D. G.; Schwertmann, U., The Influence of Aluminum on the Formation of Iron Oxides. IV.
556 The Influence of [Al], [OH], and Temperature. *Clays Clay Miner.* **1979,** *27* (3), 195-200.
557 49.   Schwertmann, U., Occurrence and Formation of Iron Oxides in Various Pedoenvironments. In
558 *Iron in Soils and Clay Minerals*, Stucki, J. W.; Goodman, B. A.; Schwertmann, U., Eds. Springer
559 Netherlands: Dordrecht, 1988; pp 267-308.
560 50.   Scheinost, A. C.; Schulze, D. G.; Schwertmann, U., Diffuse Reflectance Spectra of Al Substituted
561 Goethite: A Ligand Field Approach. *Clays Clay Miner.* **1999,** *47* (2), 156-164.
562 51.   Zhang, P.; Wu, Z.; Zhang, G.; Zeng, G.; Zhang, H.; Li, J.; Song, X.; Dong, J., Coagulation
563 characteristics of polyaluminum chlorides PAC-Al30 on humic acid removal from water. *Sep. Purif.*
564 *Technol.* **2008,** *63* (3), 642-647.

565

566

567

568

569

570

571

572